

## Molecular Physics

An International Journal at the Interface Between Chemistry and Physics

ISSN: 0026-8976 (Print) 1362-3028 (Online) Journal homepage: <https://www.tandfonline.com/loi/tmph20>

# Quantum-state-specific reaction rate measurements for the photo-induced reaction $\text{Ca}^+ + \text{O}_2 \rightarrow \text{CaO}^+ + \text{O}$

Philipp C. Schmid, Mikhail I. Miller, James Greenberg, Thanh L. Nguyen, John F. Stanton & H. J. Lewandowski

To cite this article: Philipp C. Schmid, Mikhail I. Miller, James Greenberg, Thanh L. Nguyen, John F. Stanton & H. J. Lewandowski (2019) Quantum-state-specific reaction rate measurements for the photo-induced reaction  $\text{Ca}^+ + \text{O}_2 \rightarrow \text{CaO}^+ + \text{O}$ , Molecular Physics, 117:21, 3036-3042, DOI: [10.1080/00268976.2019.1622811](https://doi.org/10.1080/00268976.2019.1622811)

To link to this article: <https://doi.org/10.1080/00268976.2019.1622811>



Published online: 28 May 2019.



Submit your article to this journal [↗](#)



Article views: 366



View related articles [↗](#)






View Crossmark data [↗](#)



Citing articles: 9 View citing articles [↗](#)

## Quantum-state-specific reaction rate measurements for the photo-induced reaction $\text{Ca}^+ + \text{O}_2 \rightarrow \text{CaO}^+ + \text{O}$

Philipp C. Schmid <sup>a</sup>, Mikhail I. Miller<sup>a</sup>, James Greenberg<sup>a</sup>, Thanh L. Nguyen <sup>b</sup>, John F. Stanton <sup>b</sup> and H. J. Lewandowski<sup>a</sup>

<sup>a</sup>JILA and the Department of Physics, University of Colorado, Boulder, Colorado, USA; <sup>b</sup>Quantum Theory Project, Departments of Chemistry and Physics, University of Florida, Gainesville, Florida, USA

### ABSTRACT

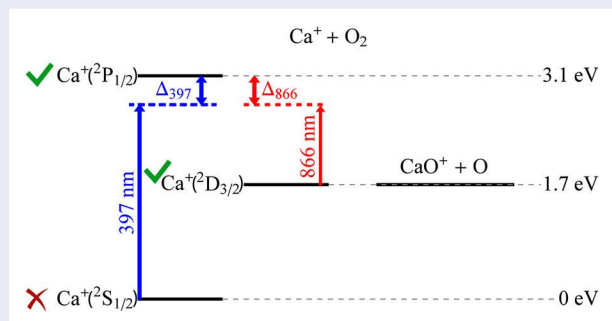
Atoms and molecules often react at different rates depending on their internal quantum states. Thus, controlling which internal states are populated can be used to manipulate the reactivity and can lead to a more detailed understanding of reaction mechanisms. We demonstrate this control of reactions by studying the electronically excited state reaction  $\text{Ca}^+ + \text{O}_2 \rightarrow \text{CaO}^+ + \text{O}$ . This reaction is exothermic only if  $\text{Ca}^+$  is in one of its excited electronic states. Using laser-cooling and electrodynamic trapping, we cool and trap  $\text{Ca}^+$  at millikelvin temperatures for several minutes. We can then change the fraction of time they spend in each of the two excited states by adjusting the detunings of the cooling lasers. This allows us to disentangle the reactions that begin with  $\text{Ca}^+$  in the  $^2\text{P}_{1/2}$ -state from the ones where  $\text{Ca}^+$  is in the  $^2\text{D}_{3/2}$ -state. Using time-of-flight mass spectrometry, we determine independent reaction rate constants for  $\text{Ca}^+$  in both electronically excited states.

### ARTICLE HISTORY

Received 30 December 2018  
Accepted 13 May 2019

### KEYWORDS

Linear ion trap; Coulomb crystals; chemical reactions; photo-assisted reaction



## 1. Introduction

The study of cold, controlled molecular reactions and collisions in the gas phase is a steadily growing field, offering many opportunities for detailed studies of interactions [1–4]. Several different experimental pathways are currently used to explore cold molecular interactions with neutral molecules. These include, but are not limited to, crossed-beam experiments using a Stark decelerator [5,6], merged-beam experiments [7,8], co-trapped atoms and molecules [9,10], buffer-gas cooled molecules inside magnetic traps [11], trapped Rydberg molecules [12], laser-cooled molecules [13–17] and ultracold bi-alkali atom molecules [18,19]. Another set of experiments uses laser-cooled atomic ions confined in radio-frequency (rf)

traps as reactants, or as a cold bath to sympathetically cool molecular ions for reaction studies [20,21].

While most of these experiments benefit from reducing the translational motion via cooling to temperatures below  $T \leq 1$  K, controlling the internal states of the reactants can offer additional insights into understanding the reactions. Preparing the reactants in a single quantum state [22–25] could elucidate the state's influence on reaction pathways. There have been some experiments that explore cold reactions where the internal states of the atomic reactant have been controlled including, but not limited to,  $\text{Ca}^+ + \text{O}_2$  [26],  $\text{Ca}^+ + \text{H}_2$  [27],  $\text{Ca}^+ + \text{H}_2\text{O}$  [28],  $\text{Ca}^+ + \text{Rb}$  [29],  $\text{Yb}^+ + \text{Rb}$  [30],  $\text{Ba}^+ + ^{87}\text{Rb}$  [31], or  $\text{Ca}^+ + (\text{CH}_3\text{F}, \text{CH}_2\text{F}_2, \text{or } \text{CH}_3\text{Cl})$  [32],

$\text{Ca}^+ + {}^6\text{Li}$  [33],  $\text{Yb}^+ + {}^6\text{Li}$  [34], and  $\text{Be}^+ + \text{H}_2\text{O}$  [35]. These experiments take advantage of the control of electronic states of the atomic ion using cooling lasers. However, preparation of pure state-selective molecular samples is significantly more challenging [12,36,37].

Here, we explore the reaction between laser-cooled  $\text{Ca}^+$  ions and neutral  $\text{O}_2$ , where the reaction can proceed only when  $\text{Ca}^+$  is in one of two excited electronic states ( ${}^2\text{P}_{1/2}$  or  ${}^2\text{D}_{3/2}$ ). We control the relative populations in the different quantum states by the wavelengths of the cooling lasers. Although the reaction of  $\text{Ca}^+ + \text{O}_2$  has been observed previously [26], no details on the reaction kinetics or the influence of the quantum states of  $\text{Ca}^+$  have been reported. In this work, we present a detailed study on the reaction  $\text{Ca}^+ + \text{O}_2 \rightarrow \text{CaO}^+ + \text{O}$ , including the absolute reaction rate constants for reactions starting with  $\text{Ca}^+$  in either the  ${}^2\text{P}_{1/2}$ -state or  ${}^2\text{D}_{3/2}$ -state.

In this paper, we begin by discussing the energetics of the reaction (Section 2) before discussing the experimental setup (Section 3). Next, we present results of the reaction measurements and the dependence of the rates on the quantum state of  $\text{Ca}^+$  (Section 4). We then discuss the implications of our results (Section 5), and conclude by giving an outlook for future experiments (Section 6).

## 2. $\text{Ca}^+ + \text{O}_2$ reactions

In the experiments presented here, we show measurements of the reactions between  $\text{Ca}^+$  ions, which have been laser-cooled to millikelvin temperatures, and  $\text{O}_2$  molecules at room temperature. This leads to an average collision energy of  $\sim 160$  K. This estimation neglects the effect of the micromotion on the collision energy. Based on the images of our ion crystals and previously published values for the temperature of similar sized crystals [38], we estimate an upper limit to the effective kinetic temperature from micromotion to be  $\langle E_{\text{eff}} \rangle / k_B < 10$  K. Although the inclusion of micromotion slightly increases the effective kinetic temperature of the ionic reactants, its value is still negligible compared to the energy of the  $\text{O}_2$  molecules.

The reaction of  $\text{Ca}^+$  with  $\text{O}_2$  is highly endothermic (+1.7 eV) when  $\text{Ca}^+$  is in the ground  ${}^2\text{S}_{1/2}$ -state [39], but becomes feasible when the excited states of the atomic cation are involved. With the  ${}^2\text{P}_{1/2}$  state, the reaction is exothermic, and for  ${}^2\text{D}_{3/2}$ , it is thermoneutral to within the accuracy of a high-level calculation. The numbers here are based on a thermochemical cycle that involves the bond energy (4.202 eV) and ionisation potential (6.895 eV) of  $\text{CaO}$ , the bond energy of  $\text{O}_2$ , and the ionisation potential and relative cation energies of the  $\text{Ca}$  atom. The numbers associated with  $\text{CaO}$  are from high-level theory, and are taken from a previous study

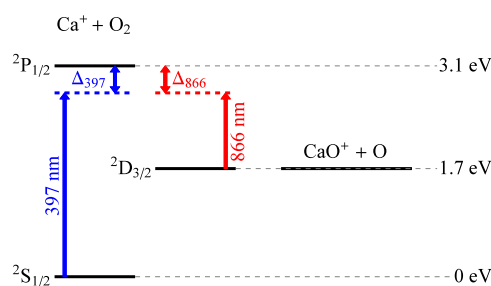
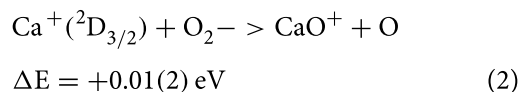
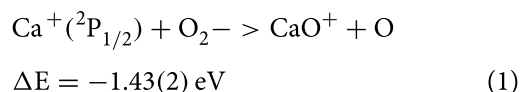


**Figure 1.** Diagram of the  $\text{Ca}^+$  energy structure and product channel energy (energies are not to scale). The main laser cooling transition for  $\text{Ca}^+$  at 397 nm excites the ion to the  ${}^2\text{P}_{1/2}$ -state. The ion can decay to the ground  ${}^2\text{S}_{1/2}$ - or the excited  ${}^2\text{D}_{3/2}$ -state. A second laser at 866 nm repumps population that accumulates in the dark  ${}^2\text{D}_{3/2}$ -state back into the cooling cycle. Here,  $\Delta_{397}$  and  $\Delta_{866}$  represent the detuning of the cooling lasers with respect to the two cooling transition frequencies. The reaction with  $\text{O}_2$  is energetically possible in either of the two excited states, but not in the ground state.

[40], while the others are precise and well-established numbers from the literature.



We note that the endothermicity of the  ${}^2\text{D}_{3/2}$ -state reaction is comparable to the uncertainty in the calculated energy. However, the collision energy is observed to be sufficient to counter this endothermicity, if indeed it is present. Thus, the reaction rate for  $\text{Ca}^+ + \text{O}_2$  will depend on the population of both excited states of  $\text{Ca}^+$ .

We control the relative populations of  $\text{Ca}^+$  in its two excited states by adjusting the detuning of both the main cooling laser at 397 nm and the repump laser at 866 nm (Figure 1). To determine the fraction of the time the  $\text{Ca}^+$  spends in each of its three electronic states, we use the 8-level optical Bloch equations (OBE) calibrated to the magnitude of the fluorescence from the Coulomb crystal following the method described in [32]. Once calibrated, the 8-level OBE are used to predict the populations in each state based on the detunings of both lasers used for laser cooling. An example set of curves for the three states is shown in Figure 2. Here, the repump laser detuning is fixed, while the main cooling laser detuning is varied.

## 3. Ion trap apparatus

Details of the experimental setup for measuring reactions between cations and neutrals have been described recently [40,41]. In the following, we present a short

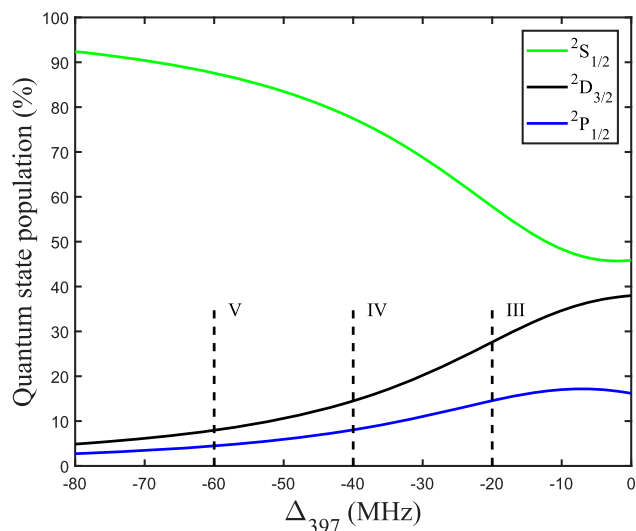


**Figure 2.** Predictions of the state distribution of the  $\text{Ca}^+$  ion from the 8-level OBE with a fixed 866 nm detuning (+42 MHz). The state populations for the  $^2\text{S}_{1/2}$ ,  $^2\text{P}_{1/2}$ , and  $^2\text{D}_{3/2}$  states are shown. The vertical lines represent the parameters used for three measurements used to determine the rate constants presented in Section 4 (see Table 1). To obtain the other state distributions shown in Table 1, we also changed the 886 nm laser detuning.

description of the apparatus with an emphasis on aspects relevant for the present experiment.

$\text{Ca}^+$  ions are created from non-resonant photoionisation of calcium atoms at 355 nm (7 mJ/pulse, 10 Hz, beam diameter  $\approx 1 \text{ mm}^2$ ) and trapped using a segmented, linear quadrupole ion trap [40]. The trapped  $\text{Ca}^+$  ions are laser cooled [42] to secular temperatures close to the Doppler cooling limit resulting in the formation of Coulomb crystals [43]. Laser cooling is performed on the  $^2\text{S}_{1/2}$ – $^2\text{P}_{1/2}$  transition, driven at 397 nm by a fibre-coupled diode laser (NewFocus, 3.5 mW, 600  $\mu\text{m}$  beam diameter). A second fibre-coupled diode laser at 866 nm (NewFocus, 9 mW, 2 mm beam diameter) is used to repump the ions back into the cooling cycle on the  $^2\text{P}_{1/2}$ – $^2\text{D}_{3/2}$  transition.<sup>1</sup> Both laser frequencies are measured and locked using a wavemeter (HighFinesse/Ångstrom WSU-30) with a precision of  $\pm 2.5 \text{ MHz}$  around the centre frequency. The wavemeter is calibrated daily to a 780 nm laser, locked to a transition in  $^{87}\text{Rb}$  by saturation absorption spectroscopy.

Detection of the trapped ions is done by two different methods. We can image the fluorescence from the Coulomb crystal onto an intensified CCD camera or eject the ions into a time-of-flight mass spectrometer (TOF-MS), which is radially coupled to the linear ion trap [40]. Optical detection has the advantage of being non-destructive, but is sensitive to only  $\text{Ca}^+$ . Non-fluorescing ions can be inferred only by a change in the shape of the Coulomb crystal in combination with

results from molecular dynamics simulations [44]. In the present experiment, we use the optical detection of pure  $\text{Ca}^+$  crystals to determine the initial number of trapped atomic ions by fitting the area of the crystal and knowing the density of ions in the trap [40]. To accurately determine the number of all trapped reactant and product ions, we eject all ions in the trap into the TOF-MS. This allows us to determine the absolute number of ions at each mass in a single shot [40]. Thus, we can study the reactions by the increase of products, as well as by the loss of reactants.

An experimental sequence starts by loading a  $\text{Ca}^+$  Coulomb crystal into the ion trap and removing any impurity ions by varying the trapping fields. Next, an image of the crystal is taken to determine the initial number of  $\text{Ca}^+$  ions. At this point,  $\text{O}_2$  is introduced into the chamber through a leak valve for a predetermined length of time. After the set reaction time has been reached, all trapped ions are ejected into the TOF-MS and a mass spectrum is produced. The total number of ions (product + reactant) is also determined from the full mass spectrum [40] at each time point to ensure the number of ions remains constant during a reaction measurement and ions are not lost from the trap. To test the conservation of ions in the trap, we sum the number of ions in every mass channel and compare this sum at each time step in the reaction to the initial number of  $\text{Ca}^+$  ions. This check is especially important when measuring the highly exothermic, excited-state reaction of  $\text{Ca}^+ + \text{O}_2$ , where the charged products may have  $> 1 \text{ eV}$  of kinetic energy.

There is one notable improvement to the apparatus compared to our previous work [40], which concerns how we introduce the neutral reactant. Instead of having the  $\text{O}_2$  present during the trap loading sequence, we now implement a pulsed-leak valve [45]. The valve consists of an all-metal leak valve (Kurt Lesker LVM series) with a 3-way solenoid valve (Parker Hannifin) connected to the input port. The 3-way valve connects the input port of the leak valve to either a roughing pump or a bottle of  $\text{O}_2$  diluted to 60% in  $\text{N}_2$ . In this configuration, the leak valve is held open at a desired leak rate at all times and the 3-way valve controls whether or not  $\text{O}_2$  flows into the chamber. Using the 3-way valve to initiate the introduction of  $\text{O}_2$  into the trapping chamber, we achieve a stable background  $\text{O}_2$  pressure in around 1–2 seconds. This time sets the uncertainty in the initial time for the reactions. We note that the pressure of  $\text{O}_2$  was measured using an ion gauge, which can give readings that are accurate to within only a factor of 2–3. This systematic will not affect the relative rates between the two states, however.

Although care is taken to introduce pure  $\text{O}_2$  gas into the vacuum chamber, there is always the possibility that

contaminants can be entrained in the gas flow. Since all trapped ions are detected in the TOF-MS spectrum simultaneously, we can measure any background reactions between  $\text{Ca}^+$  and  $\text{H}_2\text{O}$  (the dominant contaminant), which lead to the production of  $\text{CaOH}^+$ . Therefore, we can account for parasitic background reactions in our modelling of the reaction rates.

#### 4. Reaction rate constant measurements

We model the reactions in our experiment using pseudo-first-order kinetics, where we assume that the density of  $\text{O}_2$  does not change during a reaction measurement. We model the system by including reactions that start with the  $\text{Ca}^+$  in the two excited states. Equation (3) describes the growth of the charged product,  $\text{CaO}^+$ .

$$[\text{CaO}^+] = [\text{Ca}_0^+](1 - e^{-k_{\text{eff}}[\text{O}_2]t}) \quad (3)$$

Here,  $[\text{CaO}^+]$  is the number of  $\text{CaO}^+$  ions as a function of reaction time,  $t$ ,  $[\text{Ca}_0^+]$  is the initial number of trapped  $\text{Ca}^+$  ions,  $k_{\text{eff}}$  is the effective reaction rate constant, and  $[\text{O}_2]$  is the oxygen concentration in the chamber. The effective reaction rate constant,  $k_{\text{eff}}$ , is given by

$$k_{\text{eff}} = k_P f_P + k_D f_D, \quad (4)$$

where  $k_P$  ( $k_D$ ) is the rate constant for reactions with  $\text{Ca}^+$  in the P (D)-state, and  $f_P$  ( $f_D$ ) is the fraction of the  $\text{Ca}^+$  ions in the P (D)-state.

To extract the quantum-state dependent reaction rate constants, we first measure  $k_{\text{eff}}$  at several different state populations. We accomplish this by varying the detunings of the cooling lasers, while maintaining a constant  $\text{O}_2$  concentration. An example of one such rate measurement is shown in Figure 3. With our experimental parameters, the  $^2\text{P}_{1/2}$ -state population can be varied between 4% and 16%, while the  $^2\text{D}_{3/2}$ -state range is between 8% and 50%. We are not able to work outside this range, as either the heating rates become too large such that we can not maintain a stable Coulomb crystal due to the energy imparted by collisions with the background gas or the population is not possible due to the coupling in an eight-level system. A summary of the determined  $k_{\text{eff}}$  for the different state populations is given in Table 1. We perform a two-dimensional fit to these data using Equation (4) as the model to extract two fit parameters,  $k_P$  and  $k_D$ . The data and the fit can be seen Figure 4. The measurements are shown as diamond points, where the colour represents  $k_{\text{eff}}$ . The fit is shown as contour lines of constant  $k_{\text{eff}}$ . The rate constants from the fit are given in Table 2. The rate constant for  $\text{Ca}^+$  in its  $^2\text{D}_{3/2}$ -state is about three times lower than  $^2\text{P}_{1/2}$ -state reactions.

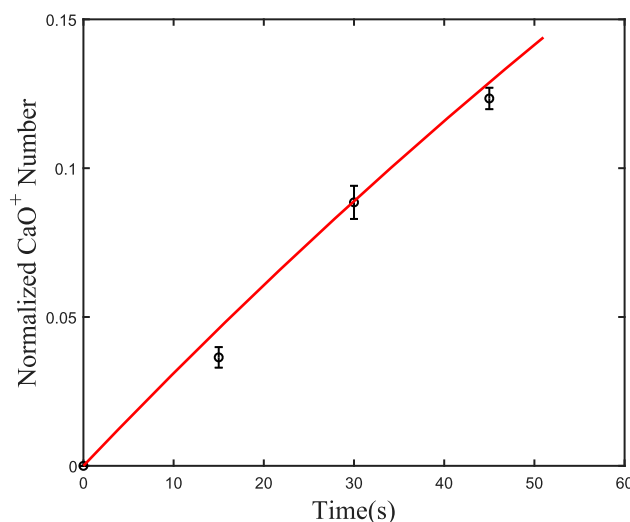


**Figure 3.** Example reaction measurement showing the growth of  $\text{CaO}^+$  product ions, normalised by the initial number of  $\text{Ca}^+$  ions ( $\sim 800$ ). The fraction in the  $^2\text{P}_{1/2}$ -state is 0.16 and  $^2\text{D}_{3/2}$ -state is 0.22, with an  $\text{O}_2$  density of  $8.9 \times 10^7 \text{ cm}^{-3}$ . The solid line is a fit using Equation (3), where  $k_{\text{eff}}$  is the only free parameter. The error bars correspond to the standard error of the mean of 7 measurements at each time point.

**Table 1.** Measured reaction rate constants for pairs of  $\text{Ca}^+$  excited state populations shown in Figure 4. The fractional populations in the  $^2\text{P}_{1/2}$ -state ( $f_P$ ) and  $^2\text{D}_{3/2}$ -state ( $f_D$ ) are shown with the corresponding measured effective rate constant ( $k_{\text{eff}}$ ). The data point numbers correspond to measurements shown in Figure 4.

Data point	$f_P$	$f_D$	$k_{\text{eff}} (10^{-11} \text{ cm}^3 \text{ s}^{-1})$
I	0.13	0.32	4.1(7)
II	0.16	0.22	3.5(4)
III	0.15	0.28	4.1(6)
IV	0.08	0.15	2.3(1)
V	0.04	0.08	1.4(1)
VI	0.07	0.50	3.6(4)

#### 5. Discussion

There are two possible explanations as to why the rate constants for the different quantum states are not the same. The first, and most likely, of these is related to the energy of the  $^2\text{D}_{3/2}$ -state. The calculated energy of the  $\text{Ca}^+(^2\text{D}_{3/2}) + \text{O}_2$  entrance channel is coincident, to within the estimated uncertainty, to that of the  $\text{CaO}^+ + \text{O}$  outgoing channel. If the reaction is indeed endothermic by an amount comparable to the collision energy, then only a portion of the Boltzmann distribution of the  $\text{O}_2$  molecules have enough energy to react. Assuming the ions are at rest and the  $\text{O}_2$  is at 300 K, the estimated collision energy is 160 K. To have a reduction of the rate constant by a factor of three (i.e. only one-third of the collisions have enough energy to react), an energy barrier of ca. 15 meV would have to exist. Given that this is

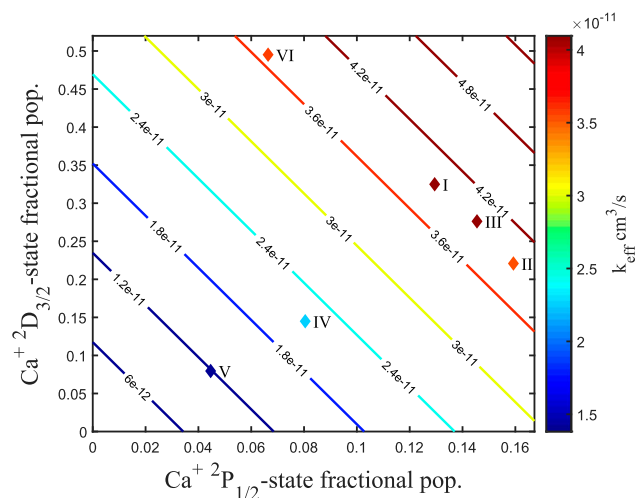


**Figure 4.** Dependence of the effective rate constant,  $k_{\text{eff}}$ , on the  ${}^2\text{P}_{1/2}$ - and  ${}^2\text{D}_{3/2}$ -state populations of  $\text{Ca}^+$ . The experimental measurements are shown as diamonds, where the colour of the point represents the value of  $k_{\text{eff}}$ . For all data shown, the  $\text{O}_2$  concentration was kept constant at  $8.9 \times 10^7 \text{ cm}^{-3}$ . We perform a two-dimensional fit to the data using Equation (4), which allows us to extract  $k_P$  and  $k_D$ . The contour lines represent constant  $k_{\text{eff}}$  values of the fit.

**Table 2.** The resulting rate constants  $k_P$  ( $k_D$ ) for the three quantum states of  $\text{Ca}^+$ . Uncertainties are from the 90% confidence interval for the fit parameters,  $k_P$  ( $k_D$ ).

$\text{Ca}^+$ state	$k$ ( $10^{-10} \text{ cm}^3 \text{ s}^{-1}$ )
${}^2\text{S}_{1/2}$	0
${}^2\text{P}_{1/2}$	1.8(4)
${}^2\text{D}_{3/2}$	0.5(2)

in quantitative agreement with the calculated energy, this is an entirely plausible explanation for the observations. However, the uncertainty in the calculation includes the possibility that the reaction is actually exothermic, so one needs to be conservative in making such an assertion.

If the possible endothermicity of the reaction involving  $\text{Ca}^+({}^2\text{D}_{3/2})$  is not the explanation for the slower rate, then a mechanistic rationalisation is needed. The association of the calcium ion and  $\text{O}_2$  will involve some sort of intermediate complex, and thus it is necessary to consider the full triatomic potential energy surface. Given that the reaction involves an excited state calcium atom, the lowest electronic states of ‘ $\text{CaO}_2^+$ ’ lay well below the energy of the entrance channel, and a reaction pathway involving many highly excited electronic states is likely. While a detailed theoretical study of such a process is well beyond the scope of this paper, some indication of the structures and electronic states involved can be gleaned from Figure 5. This displays calculated energetics obtained with coupled-cluster theory based on single, double, and perturbative triple excitations (CCSD(T))

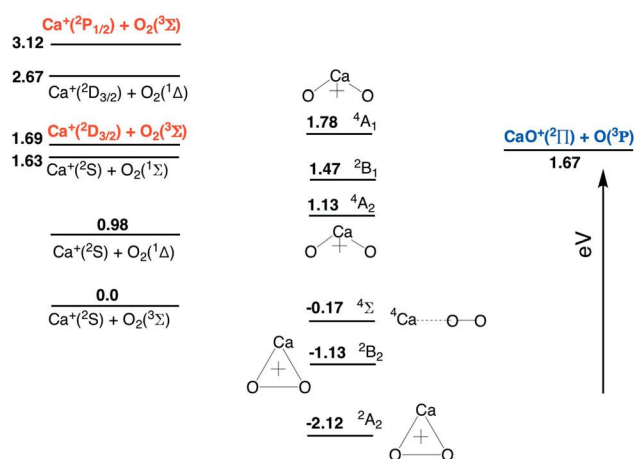


**Figure 5.** An energy-level diagram featuring electronic states of reactants, intermediates, and the observed  $\text{CaO}^+ + \text{O}({}^3\text{P})$  product channel. All energies calculated at the CCSD(T) level, apart from those levels involving excited states of molecular oxygen, that use experimental excitation energies.

[46,47] together with the cc-pCVTZ basis set [48]. This level of theory is somewhat less rigorous than that used to calculate the reaction energetics documented earlier, differences are likely small (i.e. +0.01 eV for the effectively thermoneutral channel  $v$ . -0.02 with CCSD(T)/cc-pCVTZ) and the results are expected to be accurate to within *ca.* 0.02–0.04 eV for the states shown in the figure. Only the lowest doublet and quartet states of various symmetries are shown, all of which are both *bona fide* minima on the potential energy surface and qualitatively described by a single Slater determinant (thus treated well by CCSD(T)).

Figure 5 shows that the association of  $\text{Ca}^+$  and  $\text{O}_2$  can potentially lead to states belonging to several manifolds of spin multiplicity and spatial symmetry, the lowest of which lies very far below the association asymptote. Favorable association of the  ${}^2\text{P}_{1/2}$  and  ${}^2\text{D}_{3/2}$  states of the atomic calcium ion with ground state  $\text{O}_2$  correlates with  ${}^2\text{A}_2$  and  ${}^2\text{B}_2$  states of the  $\text{C}_{2v}$  intermediate, where the former arises from pairing of in-plane electrons (forming a  $\sigma$  bond) and the latter from a  $\pi$  interaction. The lowest states of these symmetries will correlate adiabatically with  $\text{Ca}^+({}^2\text{S}) + \text{O}_2({}^3\Sigma)$ , with higher-lying  ${}^2\text{A}_2$  and  ${}^2\text{B}_2$  states correlating adiabatically with the  $\text{Ca}^+({}^2\text{P}_{1/2})$  or  ${}^2\text{D}_{3/2} + \text{O}_2({}^3\Sigma)$  reactants. The minimum-energy path for the approach of the  ${}^2\text{P}_{1/2}$  state will be in  $\text{C}_s$  symmetry on excited  ${}^2\text{A}'$  and  ${}^2\text{A}'$  surfaces that correlates with  ${}^2\text{B}_2$  and  ${}^2\text{A}_2$  states of the favoured cyclic structure, respectively; the approach of the  ${}^2\text{D}_{3/2}$ -state atomic cation is symmetry allowed in  $\text{C}_{2v}$ . Although the excited states that adiabatically correlate to reactants have not been calculated in this cursory exploration, it is likely that rapid internal conversion will produce vibrationally hot

complexes associated with the lowest two electronic states (Figure 5) that can then dissociate to observed products. Dissociation of complexes associated with these cyclic geometries would certainly encounter a barrier, but the complex will form with roughly 4–5 eV of internal energy, which should be sufficient to surmount it. However, the possibility remains that the barriers for these processes are sufficiently great that they are above the entrance channel associated with  $\text{Ca}^+ (^2D_{3/2})$ . If so, then another state of the complex that might come into play is the  $^2B_1$  state of the open form, which likely dissociates without a barrier. In such a scenario, the lower-energy entrance channel would react by a completely different pathway, and perhaps at the slower rate observed experimentally.

Note that the possibility discussed above is based on a very simple thermodynamic observation (the fact that the  $^2B_1$  intermediate lies below products) and the assumption that its dissociation to  $\text{CaO}^+$  and atomic oxygen is barrierless. Taking a theoretical investigation of the reaction process beyond this would involve a significant amount of effort; it is perhaps more productive to focus on reducing the uncertainty for the calculated reaction energy for  $\text{Ca}^+ (^2D_{3/2}) + \text{O}_2$ , the established endothermicity of which could successfully account for the difference in rate.

## 6. Summary

We measured the ionic products from the photo-induced reaction of  $\text{Ca}^+ + \text{O}_2 \rightarrow \text{CaO}^+ + \text{O}$  using laser-cooled and trapped samples of  $\text{Ca}^+$  ions. The product ions were trapped and sympathetically cooled by the atomic ions and detected using a TOF-MS. The reaction is energetically allowed only when the  $\text{Ca}^+$  is in one of two electronically excited states ( $^2P_{1/2}$  or  $^2D_{3/2}$ ). By adjusting the detunings of the cooling lasers, the quantum-state population of the  $\text{Ca}^+$  ions can be controlled. Using this control, we were able to determine reaction rate coefficients for reactions starting in either the  $^2P_{1/2}$ - or  $^2D_{3/2}$ -state. The  $^2P_{1/2}$ -state rate constant is a factor of three larger than for the  $^2D_{3/2}$ -state. We propose two possible explanations for this difference. The  $^2D_{3/2}$ -state reaction might be endothermic by a very small amount or, perhaps, proceeds through a different mechanism involving the  $^2B_1$  state of the charged  $\text{CaO}_2$  intermediate.

In future work, we plan to extend these types of measurements to more complex systems, such as reactions with organic molecules, and with additional control over the neutral reactant using a Stark decelerator. We will attach a travelling-wave Stark decelerator [49,50] to the ion trap apparatus, similar to the experiments of the Oxford group [51] and the recent proposal

by the Willitsch group [52]. This will allow us to tune the velocity of the neutral reactant down to  $10 \text{ ms}^{-1}$ , enabling studies of ion-molecule reactions below 10 K. A Stark decelerator can also produce molecules in a single quantum state, thus enabling studies of the influence of the internal molecular states on the reaction. Ultimately, by introducing state-selective molecular ions into the trap [53,54], fully quantum-state resolved molecular reactions at cold temperatures will be possible.

## Note

- $^{40}\text{Ca}^+$  has a second possible cooling scheme, which uses the  $^2S_{1/2} - ^2P_{3/2}$  transition for cooling and the  $^2P_{3/2} - ^2D_{5/2}$  transition for repumping. The two transition wavelengths – 393 nm and 854 nm – are not within the bandwidth of our laser systems. We therefore neglect these electronic states for the scope of this work.

## Disclosure statement

No potential conflict of interest was reported by the authors.

## Funding

This work was supported by the National Science Foundation (Division of Physics PHY-1734006, CHE-1664325, and Division of Chemistry CHE-1464997), Air Force Office of Scientific Research (AFOSR) (FA9550-16-1-0117), and National Institute of Standards and Technology (NIST).

## ORCID

Philipp C. Schmid  <http://orcid.org/0000-0002-1644-0495>

Thanh L. Nguyen  <http://orcid.org/0000-0002-7794-9439>

John F. Stanton  <http://orcid.org/0000-0003-2345-9781>

## References

- O. Dulieu and C. Gabbanini, *Rep. Prog. Phys.* **72**, 086401 (2009).
- O. Dulieu and A. Osterwalder, *Cold Chemistry*, Theoretical and Computational Chemistry Series (The Royal Society of Chemistry, Cambridge, 2018), pp. P001–670.
- L.D. Carr, D. DeMille, R.V. Krems and J. Ye, *New J. Phys.* **11**, 055049 (2009).
- J.M. Doyle, B. Friedrich and E. Narevicius, *Chem. Phys. Chem.* **17**, 3581 (2018).
- S.N. Vogels, J. Onvlee, S. Chefdeville, A. van der Avoird, G.C. Groenenboom and S.Y.T. van de Meerakker, *Science* **350**, 787 (2015).
- Z. Gao, T. Karman, S.N. Vogels, M. Besemer, A. van der Avoird, G.C. Groenenboom and S.Y.T. van de Meerakker, *Nat. Chem.* **10**, 469 (2018).
- A. Klein, W.S. Yuval Shagam, M.P. Piotr, S. Żuchowski, N.M. Liesbeth, M.C. Janssen, S.Y.T. van de Meerakker, A. van der Avoird, C.P. Koch and E. Narevicius, *Nat. Chem.* **13**, 35 (2017).
- S.D.S. Gordon, J. Zou, S. Tanteri, J. Jankunas and A. Osterwalder, *Phys. Rev. Lett.* **119**, 053001 (2017).

- [9] L.P. Parazzoli, N.J. Fitch, P.S. Żuchowski, J.M. Hutson and H.J. Lewandowski, *Phys. Rev. Lett.* **106**, 193201 (2011).
- [10] N. Akerman, M. Karpov, Y. Segev, N. Bibelnik, J. Narevicius and E. Narevicius, *Phys. Rev. Lett.* **119**, 073204 (2017).
- [11] J.D. Weinstein, T. Guillet, B. Friedrich, J.M. Doyle and R. deCarvalho, *Nature* **395**, 148 (1998).
- [12] P. Allmendinger, J. Deiglmayr, O. Schullian, K. Höveler, J.A. Agner, H. Schmutz and F. Merkt, *ChemPhysChem* **17**, 3596 (2016).
- [13] L. Anderegg, B.L. Augenbraun, E. Chae, B. Hemmerling, N.R. Hutzler, A. Ravi, A. Collopy, J. Ye, W. Ketterle and J.M. Doyle, *Phys. Rev. Lett.* **119**, 103201 (2017).
- [14] I. Kozryyev, L. Baum, K. Matsuda, B.L. Augenbraun, L. Anderegg, A.P. Sedlack and J.M. Doyle, *Phys. Rev. Lett.* **118**, 173201 (2017).
- [15] E.B. Norrgard, D.J. McCarron, M.H. Steinecker, M.R. Tarbutt and D. DeMille, *Phys. Rev. Lett.* **116**, 063004 (2016).
- [16] H.J. Williams, S. Truppe, M. Hambach, L. Caldwell, N.J. Fitch, E.A. Hinds, B.E. Sauer and M.R. Tarbutt, *New J. Phys.* **19**, 113035 (2017).
- [17] M.T. Hummon, M. Yeo, B.K. Stuhl, A.L. Collopy, Y. Xia and J. Ye, *Phys. Rev. Lett.* **110**, 143001 (2013).
- [18] T. Kraemer, M. Mark, P. Waldburger, J. Danzl, C. Chin, B. Engeser, A. Lange, K. Pilch, A. Jaakkola, H.-C. Nägerl and R. Grimm, *Nature* **440**, 315 (2006).
- [19] S. Ospelkaus, K.-K. Ni, D. Wang, M.H.G. de Miranda, B. Neyenhuis, G. Quémener, P.S. Julienne, J.L. Bohn, D.S. Jin and J. Ye, *Science* **327**, 853 (2010).
- [20] S. Willitsch, *Int. Rev. Phys. Chem.* **31**, 175 (2012).
- [21] B.R. Heazlewood and T.P. Softley, *Annu. Rev. Phys. Chem.* **66**, 475 (2015).
- [22] X. Tong, A.H. Winney and S. Willitsch, *Phys. Rev. Lett.* **105**, 143001 (2010).
- [23] P.F. Staunum, K. Højbjerg, P.S. Skyt, A.K. Hansen and M. Drewsen, *Nat. Phys.* **6**, 271 (2010).
- [24] T. Schneider, B. Roth, H. Duncker, I. Ernsting and S. Schiller, *Nat. Phys.* **6**, 275 (2010).
- [25] C.-Y. Lien, S.R. Williams and B. Odom, *Phys. Chem. Chem. Phys.* **13**, 18825 (2011).
- [26] M. Drewsen, L. Hornekr, N. Kjrgaard, K. Mlhve, A.-M. Thommesen, Z. Videsen, A. Mortensen and F. Jensen, *AIP Conf. Proc.* **606**, 135 (2002).
- [27] N. Kimura, K. Okada, T. Takayanagi, M. Wada, S. Ohtani and H.A. Schuessler, *Phys. Rev. A* **83**, 033422 (2011).
- [28] K. Okada, M. Wada, L. Boesten, T. Nakamura, I. Katayama and S. Ohtani, *J. Phys. B* **36**, 33 (2003).
- [29] F.H.J. Hall, M. Aymar, N. Bouloufa-Maafa, O. Dulieu and S. Willitsch, *Phys. Rev. Lett.* **107**, 243202 (2011).
- [30] L. Ratschbacher, C. Zipkes, C. Sias and M. Köhl, *Nat. Phys.* **8**, 649 (2012).
- [31] F.H. Hall, M. Aymar, M. Raoult, O. Dulieu and S. Willitsch, *Mol. Phys.* **111**, 1683 (2013).
- [32] A.D. Gingell, M.T. Bell, J.M. Oldham, T.P. Softley and J.N. Harvey, *J. Chem. Phys.* **133**, 194302 (2010).
- [33] R. Saito, S. Haze, M. Sasakawa, R. Nakai, M. Raoult, H. Da Silva, O. Dulieu and T. Mukaiyama, *Phys. Rev. A* **95**, 032709 (2017).
- [34] J. Joger, H. Fürst, N. Ewald, T. Feldker, M. Tomza and R. Gerritsma, *Phys. Rev. A* **96**, 030703 (2017).
- [35] T. Yang, A. Li, G.K. Chen, C. Xie, A.G. Suits, W.C. Campbell, H. Guo and E.R. Hudson, *J. Phys. Chem. Lett.* **9**, 3555 (2018).
- [36] X. Tong, T. Nagy, J.Y. Reyes, M. Germann, M. Meuwly and S. Willitsch, *Chem. Phys. Lett.* **547**, 1 (2012).
- [37] Y.-P. Chang, K. Długołeckı, J. Küpper, D. Rösch, D. Wild and S. Willitsch, *Science* **342**, 98 (2013).
- [38] M.T. Bell, A.D. Gingell, J.M. Oldham, T.P. Softley and S. Willitsch, *Faraday Discuss.* **142**, 73 (2009).
- [39] S. Lias, in *Nist chemistry webbook*, NIST standard reference database number 69, (National Institute of Standards and Technology, Gaithersburg MD, 20899, 2018) Chap. Ionization energy evaluation.
- [40] P.C. Schmid, J. Greenberg, M.I. Miller, K. Loeffler and H.J. Lewandowski, *Rev. Sci. Ins.* **88**, 123107 (2017).
- [41] J. Greenberg, P.C. Schmid, M. Miller, J.F. Stanton and H.J. Lewandowski, *Phys. Rev. A* **98**, 032702 (2018).
- [42] J. Eschner, G. Morigi, F. Schmidt-Kaler and R. Blatt, *J. Opt. Soc. Am. B* **20**, 1003 (2003).
- [43] M. Drewsen, *Phys. B* **460**, 105 (2015). Special Issue on Electronic Crystals (ECRYS-2014).
- [44] K. Okada, M. Ichikawa, M. Wada and H.A. Schuessler, *Phys. Rev. Appl.* **4**, 054009 (2015).
- [45] C.Q. Jiao, D.R.A. Ranatunga, W.E. Vaughn and B.S. Freiser, *J. Am. Soc. Mass Spectrom.* **7**, 118 (1996).
- [46] R.J. Bartlett, J. Watts, S. Kucharski and J. Noga, *Chem. Phys. Lett.* **165**, 513 (1990).
- [47] K. Raghavachari, G.W. Trucks, J.A. Pople and M. Head-Gordon, *Chem. Phys. Lett.* **157**, 479 (1989).
- [48] T.H. Dunning, *J. Chem. Phys.* **90**, 1007 (1989).
- [49] M.I. Fabrikant, T. Li, N.J. Fitch, N. Farrow, J.D. Weinstein and H.J. Lewandowski, *Phys. Rev. A* **90**, 033418 (2014).
- [50] Y. Shyur, J.A. Bossert and H.J. Lewandowski, *J. Phys. B* **51**, 165101 (2018).
- [51] J.M. Oldham, *Combination of a Cold Ion and Cold Molecular Source*, Ph.D. thesis, Oxford University, UK, 2014.
- [52] P. Eberle, A.D. Dörfler, C. von Planta, K. Ravi, D. Haas, D. Zhang, S.Y.T. van de Meerakker and S. Willitsch, *J. Phys.* **635**, 012012 (2015).
- [53] N.V. Vitanov, A.A. Rangelov, B.W. Shore and K. Bergmann, *Rev. Mod. Phys.* **89**, 015006 (2017).
- [54] T.J. Barnum and R.W. Field, Preparation of state selected ions, 2018 (private communication).